

COMPARING ANALYTICAL AND MACHINE-LEARNING-BASED DESIGN METHODS FOR SLENDER SECTION STEEL MEMBERS IN FIRE

Carlos Couto¹, Qi Tong², Thomas Gernay³

ABSTRACT

In thin-walled steel members, the complexity of the interaction between the buckling of the plates and the buckling of the member, combined with the reduction of steel properties with increasing temperature, hinders the development of simple accurate analytical models. As a result, analytical design methods tend to be overly conservative for simple situations, and inexistent for more complex situations such as temperature gradients and systems-level response, leading to unreliable fire design methods and affecting the attractiveness of these structures that are designed with optimization in mind. Meanwhile, data-based approaches using Machine Learning (ML) techniques have allowed overcoming complex nonlinear problems in various engineering disciplines. ML may provide fast models surpassing existing analytical methods and achieving accuracy similar to Finite Element-based solutions at much lower computational cost. While the development of ML models requires sophisticated modelling and large datasets, which may not always be available, once a ML model is developed its application to practical design situations within the limits of its validity is straightforward. This paper investigates opportunities from application of ML methods to the problem of thin-walled steel members in fire, including critical comparison of benefits and capabilities between ML methods and existing analytical approaches. With a dataset of 2304 data points for columns and 24516 for beams, the paper shows that ML models can outperform current state-of-the-art analytical models in terms of agreement with high-fidelity shell FE results.

Keywords: Machine learning; Thin-walled members; Fire; Temperature; Shell finite elements; Instability

1 INTRODUCTION

Structures made of thin-walled steel members are widely used, from highly optimized portal frames to structural systems such as light-steel framing. Their exceptional weight-to-strength ratio provides an appealing solution from the cost and material savings point of view. However, these structural members are susceptible to local buckling, a failure mode that can greatly reduce the load bearing capacity of the members. The added complexity resulting from the interaction between local buckling of the plates at the cross-section level and buckling of the member (i.e., flexural buckling and lateral torsional buckling) has hindered the development of more economic yet safe analytical design methods, which goes counter to the advantage of thin-walled members as a means to optimize design and material use. While analytical methods derived from mechanics-based principles and experimental observations are very useful for design, they are necessarily based on simplifying assumptions that lead to conservatism. Further improving their accuracy requires increasing their level of complexity, for example in the form of additional buckling curves for local and/or global buckling, which affects the practicality and makes user mistakes more likely for use as design methods.

¹ Assistant Researcher, RISCO, Civil Engineering Department, University of Aveiro, Portugal
e-mail: ccouto@ua.pt, ORCID: <https://orcid.org/0000-0003-0865-2225>

² PhD Student, Department of Civil and Systems Engineering, Johns Hopkins University, Baltimore, USA
e-mail: qtong5@jhu.edu

³ Assistant Professor, Department of Civil and Systems Engineering, Johns Hopkins University, Baltimore, USA
e-mail: tgermay@jhu.edu, ORCID: <https://orcid.org/0000-0002-3511-9226>

Stemming from possible failure due to local buckling, Finite Element (FE)-based solutions require more complex models at higher cost. Traditional beam FE models are unable to capture the effects of local buckling thus shell finite models must be used. These complex models are cumbersome to use in a daily basis, since not only the calculation cost is much higher but also the modelling part is harder and time-consuming. Although efforts to enhance the beam FE-based models to include the reduction in capacity due to local buckling were developed [1,2] these techniques are still in their infancy.

Meanwhile, data-based approaches using Machine Learning (ML) techniques have allowed overcoming complex nonlinear problems in many engineering disciplines. ML may provide fast models surpassing analytical methods and achieving accuracy close to that of FE models at much lower computational cost. This has recently led to interest towards their application for the case of structures in fire [3].

This paper investigates the development and application of ML techniques for predicting the capacity of thin-walled columns and beams at elevated temperatures. To construct the ML models, datasets are generated for elevated temperature failure of thin-walled columns and beams using a numerical model with shell finite elements in the software SAFIR [4]. Training of artificial neural networks, support vector machines and polynomial regression is carried out using established numerical methods. The outputs of the ML model are then compared against those from SAFIR and from Eurocode 3 analytical methods.

2 ANALYTICAL MODELS

2.1 Effective cross-section

For slender steel columns under compression, the evaluation of load carry capacity at elevated temperature must consider the effect of local buckling. Part 1.5 of Eurocode 3 provides expressions of reduction factors for plate buckling resistance under compression, based on the concept of effective width method accounting for geometric imperfection and residual stresses [5]. Couto et al. [6] proposed an updated formula to account for the local buckling of slender steel members (Class 3 and Class 4) at elevated temperature and replaced the use of design yield strength corresponding to the 0.2% proof strength with the yield strength at 2% total strain for Class 4.

The effective width of plates at elevated temperature can be calculated as:

$$b_{eff} = \rho_{\theta} \times b \quad (1)$$

The new expression [6] for a plate reduction factor of internal compression elements is:

$$\rho_{\theta} = \frac{(\bar{\lambda}_p + \alpha_{\theta})^{\beta_{\theta}} - 0.055(3 + \psi)}{(\bar{\lambda}_p + \alpha_{\theta})^{2\beta_{\theta}}} \leq 1.0 \quad (2)$$

For outstand compression element it is:

$$\rho_{\theta} = \frac{(\bar{\lambda}_p + \alpha_{\theta})^{\beta_{\theta}} - 0.188}{(\bar{\lambda}_p + \alpha_{\theta})^{2\beta_{\theta}}} \leq 1.0 \quad (3)$$

$\bar{\lambda}_p$ is the non-dimensional slenderness of a plate given by:

$$\bar{\lambda}_p = \frac{b/t}{28.4\epsilon\sqrt{k_{\sigma}}} \quad (4)$$

where k_{σ} is the buckling coefficient of plates, b and t are the width and thickness of the plates, ψ is the stress ratio between two ends. Coefficients α_{θ} and β_{θ} are given in Table 2 of the paper by Couto et al. [6] for internal compression elements (web) and outstand compression elements (flanges). ϵ is calculated as:

$$\epsilon = \sqrt{\frac{235}{f_y}} \sqrt{\frac{E}{210000}} \text{ in which } f_y \text{ and } E \text{ in Mpa} \quad (5)$$

According to the current Eurocode 3 Part 1-2, the effective section is determined for $\alpha_{\theta} = 0$ and $\beta_{\theta} = 1$.

2.2 Buckling of columns and beams

Once the effective width of the plates is calculated and the effective properties of the section determined, the load-carrying capacity of the members can be evaluated by making allowance for the flexural buckling or lateral-torsional buckling in the columns and beams using equations (6a) or (6b), respectively.

$$N_{b,fi,t,Rd} = \chi_{fi} \cdot A_{eff} \cdot k_{y,\theta} \cdot f_y / \gamma_{M,fi} \quad (6a)$$

$$M_{b,fi,t,Rd} = \chi_{LT,fi} \cdot W_{eff} \cdot k_{y,\theta} \cdot f_y / \gamma_{M,fi} \quad (6b)$$

where A_{eff} and W_{eff} are the effective section area and effective sections modulus, k_θ is the reduction factor for the yield strength at elevated temperatures, f_y is the yield strength, $\gamma_{M,fi}$ is the safety factor taken as 1.0. According to the present version of the Eurocode 3 Part 1-2, for Class 4 sections, $k_{y,\theta}$ is taken as the reduction factor for the 0.2% proof strength of steel at elevated temperatures ($k_{p,0.2,\theta}$).

For the columns, the buckling reduction factor for flexural buckling χ_{fi} is calculated as:

$$\chi_{fi} = \frac{1}{\phi_\theta + \sqrt{\phi_\theta^2 - \bar{\lambda}_\theta^2}} \quad \text{and} \quad \chi_{fi} \leq 1.0 \quad (7)$$

$\bar{\lambda}_\theta$ is the non-dimensional slenderness at elevated temperature and ϕ_θ is calculated as:

$$\phi_\theta = 0.5 \left[1 + \alpha(\bar{\lambda}_\theta - \lambda_0) + \bar{\lambda}_\theta^2 \right] \quad (8)$$

$\lambda_0 = 0$ and with α is the imperfection factor calculated as:

$$\alpha = 0.65\varepsilon = 0.65\sqrt{235/f_y} \quad (9)$$

The non-dimensional slenderness at elevated temperature $\bar{\lambda}_\theta$ is calculated as:

$$\bar{\lambda}_\theta = \sqrt{\frac{A_{eff} f_y k_{y,\theta}}{k_{E,\theta} N_{cr,20}}} \quad (10)$$

where $k_{E,\theta}$ is the reduction factor for Young's modulus at elevated temperatures, and $N_{cr,20}$ is the elastic critical capacity at ambient temperature.

For beams, the same procedure given by equations (7)-(10) is used to calculate the lateral-torsional buckling reduction factor $\chi_{LT,fi}$ with the subscript "LT" added to the parameters. However, α_{LT} and λ_0 take different values for beams with Class 4 cross-sections in the new generation of the Eurocode 3 Part 1-2, with the values proposed given by Couto et al. [7]. A modification factor "f" is also included to take into account the non-uniform bending diagrams as detailed in [8], and the non-dimensional slenderness is calculated as a function of the section resistance to major-axis bending and the elastic critical moment.

3 NUMERICAL MODEL AND DATASET

3.1 Finite element model

Numerical modelling was used to analyse members made of I-shaped slender cross-sections subjected to axial compression and major-axis bending at elevated temperatures. The numerical models were built using shell elements in the nonlinear finite element software SAFIR [4]. Columns and beams with different plate slenderness, lengths and, for the case of beams, end-moment ratios were modelled. The structural members were uniformly heated on four sides. Pinned or fixed support conditions, on the columns, and fork-supports on the beams were considered. A sensitivity analysis on the mesh size was conducted to have a sufficiently refined mesh while preserving an appropriate computational cost.

The constitutive model included in the simulations followed the non-linear stress-strain relationship and reduction factors defined in Eurocode 3 Part 1-2 [9]. Steels with grades S235, S355, and S460 at ambient temperature were used in the numerical models. Young's modulus of elasticity at ambient temperature was taken as 210 GPa and Poisson's ratio as 0.30.

Both geometric imperfections and material imperfections, in the form of residual stresses, were included in the models. For global imperfection, the amplitude followed the design recommendation, i.e. $L/1000$, where L is the length of the member. For local imperfection, the amplitude was calculated as 80% of the geometric fabrication tolerances [10]. The global imperfection and local imperfection were combined following the recommendation of Annex C in Part 1-5 of Eurocode 3 [5]. In accordance with the recommendations of this Annex, the full amplitude was considered for the leading imperfection while that of the accompanying imperfections was reduced to 70%. For the residual stresses, the pattern included in the models followed the one for hot-rolled columns and welded beams [10].

For columns, two rigid 100 mm thick endplates were added at both ends of the column. The load was axially applied on the edge of the vertical plate on the top with no eccentricity such that the load can be distributed evenly on the web and flange. The displacements of two rigid extensions were constrained except for the vertical direction on the top (U_y) which was left free to allow free thermal expansion. The rotations of two rigid extensions were either fixed or pinned in R_x , R_y , and R_z directions (see Figure 1).

For beams, fork-supports were used at both ends of the structural member to prevent the displacements in x -direction and y -direction. To prevent rigid body movement, the displacements in z -direction were constrained at mid-span. The loading was applied by nodal forces to produce end-moments at both ends. Additionally, end-plates were included with a thickness equal to 10 times the web thickness to ensure correct load distribution.

The ultimate load-bearing capacity of the columns was calculated with SAFIR considering steady-state conditions i.e., by first uniformly increasing the temperature in the section up to the target value and then progressively loading the members until failure was reached.

An example of the collapse shape of a IPE500 column and the corresponding boundary conditions are provided in Figure 1. More details about the numerical model can be found in [11,12].

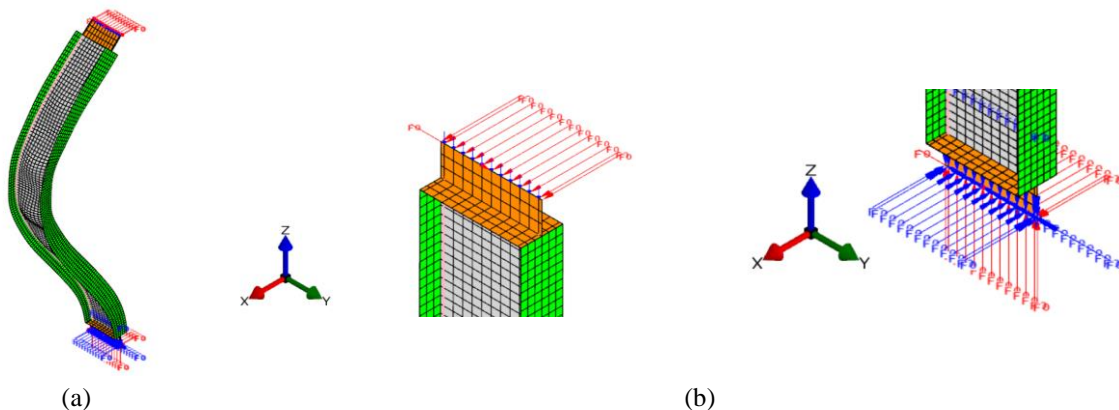


Figure 1. Numerical model in SAFIR: (a) shell model for IPE500 column at 300 °C and (b) boundary conditions with end plates and pinned-fixed supports.

3.2 Datasets

Two datasets were defined comprising respectively the column and beam cases. For each dataset, the data points were calculated using the numerical model described in the previous section. FE simulations were run to failure. The dataset includes 2304 FE simulations for the columns and 24516 for the beams. For the latter, the same data were used to develop the design rules for the lateral-torsional buckling of beams with slender section [7,8] present in new generation of the Eurocode 3 Part 1-2 and given in Section 2.

The selection of features was carried out using a procedure that combined prior knowledge about the parameters potentially influencing the mechanical response (mechanistic-informed) and a quantitative trial-and-error approach to find the most suitable combination of features. The process of feature selection dealt with both inclusion and exclusion of parameters and their combination, and the best model was selected as the one with fewest parameters for a given accuracy. The ranges of values for the input parameters are listed in Table 1 and Table 2 for columns and beams, respectively, each defining 9 and 8 features for the ML models. Similar features are defined for both cases but with a different order because the ML models

originate from two different studies by the authors [11,12]. The order of the features has no influence in the performance of the models.

Table 1. Input parameters for the ML models and for the unseen experimental dataset – columns.

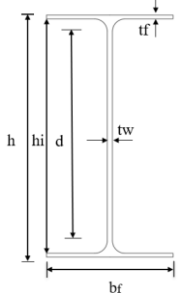
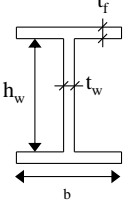
Notation	Feature	Input values	Numerical dataset		Unseen experiment dataset	
			Min.	Max.	Min.	Max.
	x_1	h_w/t_w	31	52	11.2	50
	x_2	$b_f/2t_f$	4.6	8.2	6.25	15.3
	x_3	d/b_f	0.56	2.34	0.56	2
	x_4	t_w/t_f	0.56	1	0.625	1
	x_5	$f_{y_{web}}/E$	(235/E)	(460/E)	(321.9/E)	(538.1/E)
	x_6	$f_{y_{flange}}/E$	(235/E)	(460/E)	(306.3/E)	(538.1/E)
	x_7	L/b_f	6.7	30	6.8	18.4
	x_8	$(N_{pl,20}/N_{cr,20})^{0.5}$	0.17	2.01	0.17	1.05
	x_9	<i>temperature</i>	300°C	800°C	400°C	700°C

Table 2. Input parameters/features of dataset used for the ML models training – beams.

Notation	Feature	Input values	Min.	Max.
	x_1	h_w/t_w	75	200
	x_2	b/t_f	6	50
	x_3	h_w/b	1.8	3.33
	x_4	t_w/t_f	0.16	0.8
	x_5	f_y/E	(235/E)	(460/E)
	x_6	<i>temperature</i>	300°C	700°C
	x_7	$(M_{pl,20}/M_{cr,20})^{0.5}$	0.097	2.738
	x_8	ψ	-1	1

In these tables, the h_w/t_w and $b_f/2t_f$ are the adimensional web and flange dimensions – note that for beam cases b_f/t_f was considered instead, $F_{y_{web}}/E$, $F_{y_{flange}}/E$ are the adimensional web and flange yield strengths considered for columns and f_y/E is the adimensional yield strength for beams. The L is member length, $N_{pl,20}$ and $M_{pl,20}$ are the section plastic capacity for the column and beam, $N_{cr,20}$ and $M_{cr,20}$ are their elastic critical load at ambient temperature and ψ is the ratio between end-moments applied to beams. The range of feature values considered in the dataset was chosen to cover a common range of design parameters for slender section steel columns and beams in building structures.

The output was defined as $y = N_{u,T}/N_{pl,20}$ with $N_{u,T}$ being the ultimate capacity of a column or $y = M_{u,T}/M_{pl,20}$ with $M_{u,T}$ being the ultimate capacity of a beam.

For columns, in addition to the 2304 numerical data points, 16 experiments on steel columns at elevated temperature were identified from the literature, on axially compressed stud columns with Class 4 cross-sections [13] and on pin-supported steel columns with HEA 100 cross-sections [14]. These experiments were used to test a posteriori the ability of the trained ML models to predict the outcome of the experiments, where the experimental data had not been used in the construction of the ML models. In particular, Table 1 shows that the values of the features for these 16 experimental data points (column “unseen experiment dataset”) did not always fit within the boundaries of the feature values used for training and testing the ML models. Consideration of these experiments therefore enables exploring the limits of the data-based approach when extrapolating outside the range of parameters “seen” by the model.

For the column cases, the 2304 data points were randomly divided into two groups with a ratio of 9:1, thus 2073 data points were used for training the ML models and 231 data points were used for testing the ML models. For the beam cases, the 24516 samples were divided on a proportion of 7:3, thus 17161 cases were considered for training and 7355 cases for testing.

4 MACHINE LEARNING MODELS

4.1 Artificial Neural Networks

The artificial neural network (ANN) is a mathematical model that can be described as a group of neurons arranged in layers and their connections forming a network. The ANN can map a certain range of input values (features) to a specific target value (result). The most used type of ANN is the Multilayer Perceptron (MLP), with an input layer, one or more hidden layers, and an output layer. Each neuron of a certain layer is only connected to the neurons in the next layer, and may include an extra, independent, value called the bias. The output of each neuron j can be calculated as:

$$output_j = f\left(\sum_{i=1}^n w_{ij}x_i + b_j\right) \quad (11)$$

where $output_j$ is the output of the layer, w_{ij} are the weight coefficients, x_i are the input values, or features, and b_j is the bias values. The $f(x)$ is the so-called transfer or activation function.

Then, the training of ANN is achieved by exposing the network to a set of examples (input patterns) with known outputs (target output). The weights of the internal connections, and the bias values of the neurons, are adjusted to minimize errors between the network output and target output.

Two implementations of the ANN were considered in this study, the one available in the scikit-learn [15] was used for both column and beam cases and *pyrenn* [16] was also considered for the beam case. Regarding the loss function, the *scikit-learn toolkit* implements the square error loss function in the MLP for regression, while the *pyrenn toolkit* used the mean square error loss function.

The hyperparameters were determined by the functionality of a randomized search with the cross-validation of 25 and 5 folds using the *scikit-learn toolkit* for column and beam cases, respectively. The results show that the optimal hidden layer size was 8 with the applied weight optimizer ‘lbfgs’. For the beam model, using the ‘adam’ optimizer the hidden layer size was 64. Using the Levenberg-Marquardt (LM) the hidden layer was reduced to 16 neurons and since no cross-validation was available in *pyrenn* the network architecture was manually fine-tuned.

4.2 Support Vector Machines Regression

SVR is developed as an extension of the support vector machine (SVM), which aims to find a hyperplane in an n -dimensional space (n is the number of features, i.e. input parameters) that classifies the training datasets in different classes. While the objective of SVM is to find a hyperplane that has the maximum margins ($\pm\epsilon$), the extension SVR aims to find a flat hyperplane with margins ($\pm\epsilon$) that accept the data points within or on the margins while rejecting the data points outside the margins.

The hyperplane can be written in Equation (12) for linear SVR:

$$y_i = w^T x_i + b \quad (12)$$

in which x_i and y_i are the i th input and output in the training dataset, w is the weight matrix, b is the bias. For nonlinear SVR, the hyperplane can be written as:

$$y_i = w^T \varphi(x_i) + b \quad (13)$$

in which $\varphi(x_i)$ is the nonlinear kernel function that maps the input vectors to a higher dimension space. The deviation of points within the margins ($\pm\epsilon$) is zero. The deviation of points outside the margins ($\pm\epsilon$) is the distance of these points to the margins (ξ_i and ξ_i). The loss function of SVR is written as:

$$\text{minimize: } \frac{1}{2} \|w\|^2 + C \sum_{i=1}^n (\xi_i + \xi_i) \quad (14)$$

The constraints are:

$$\begin{aligned} y_i - wx_i - b &\leq \epsilon + \xi_i \\ wx_i + b - y_i &\leq \epsilon + \xi_i \\ \xi_i, \xi_i &\geq 0 \end{aligned} \quad (15)$$

in which $\frac{1}{2} \|w\|^2$ is the regularization term added to seek the flattest hyperplane with a small weight. C is a trade-off between the accepted tolerance of deviation ε and the flatness of the solution.

The samples for training and testing are the same as for the ANN. Grid search is applied to tune the hyperparameters. The following values are used for the hyperparameters for the beam: ‘rbf’ kernel, $C=1000$, $\gamma=0.049$, and $\varepsilon = 0.05$. The following values are used for the columns: ‘rbf’ kernel, $C=82$, $\gamma=0.263$, and $\varepsilon = 0.01$.

4.3 Polynomial regression

The general form for polynomial regression is written as:

$$Y = X\omega + \varepsilon \quad (16)$$

in which Y is the vector of responses, X is the feature matrix, ω is the coefficient and ε is the bias. The polynomial regression extends the inputs of the linear model, which is obtained by raising the initial inputs to a power. The new inputs are created with degrees less than or equal to the specific order. The new feature matrix includes 1) bias; 2) converting the initial inputs to their higher-order terms for each degree; 3) combination of all pairs of initial inputs. For instance, if there are two inputs, $[x_1, x_2]$, a degree-2 polynomial expansion would produce a new feature matrix $[1, x_1, x_2, x_1^2, x_1x_2, x_2^2]$.

Models with higher degrees may closely fit most of the data in the training dataset, but possibly at the cost of over-fitting resulting in a larger error on the testing dataset. To prevent over-fitting in polynomial regression, ridge regression is applied to fit the polynomial feature matrix. The ridge regression adds a regularization term to the sum of squares of residuals. The loss function of ridge regression is written as:

$$\text{minimize: } \sum_{i=1}^n \|y_i - \sum_{j=0}^m x_{ij}w_j\|^2 + \lambda \sum_{j=0}^m \|w_j\|^2 \quad (\lambda > 0) \quad (17)$$

in which the y_i is the known observation, $\sum_{j=0}^m x_{ij}w_j$ is the predicted value, and λ is the tuning parameter which controls the complexity of the model. As λ grows larger, the ridge regression effectively shrinks coefficient w_j to be 0 and selects a small subset of features to build the model, which prevents training a more complex model and thus avoid over-fitting.

For the column, a degree 2 polynomial was found to predict the resistance of columns within the range of features provided in Table 1 of the numerical dataset. The coefficients of the degree 2 polynomial model are given in [11]. This model implemented in a datasheet can provide an almost-immediate prediction of the elevated temperature capacity for slender steel columns, within the range of features considered. For the beam, the model of degree 6 shows the best performance for both training and testing [12].

5 RESULTS AND DISCUSSION

To quantify the performance of the different models, the coefficient of determination R^2 value was evaluated for the models against the training and testing dataset and the unseen experimental data. The R^2 measures how well the observations are replicated by a model and a R^2 close to 1 is preferred. Table 3 gives the results for the SVR, ANN, and PR models for columns and beams respectively. Predictions by the analytical model described in Section 2 are also included.

Table 3. Performance of the ML models and the analytical model.

Regressor (R^2)	Columns			Beams	
	Train	Test	Unseen Experiment	Train	Test
SVR	0.998	0.996	-0.212	0.987	0.987
ANN	0.990	0.990	0.891	0.999	0.999
PR	0.980	0.977	0.914	0.981	0.981
EN1993-1-2:2005		0.928			0.829
EN 1993-1-2 New Gen.		0.956			0.963

Figure 2 (a)-(d) plots the predicted capacity $N_{u,T}/N_{pl,20}$ using SVR, ANN, PR, and the analytical models against the numerical estimations from the shell finite element model in SAFIR for the columns. For the

training and testing dataset, the results from SVR, ANN, and PR agree better with the capacity evaluated by SAFIR than the analytical model. The ANN and PR models are also able to predict the capacity in the unseen experimental datasets with good agreement.

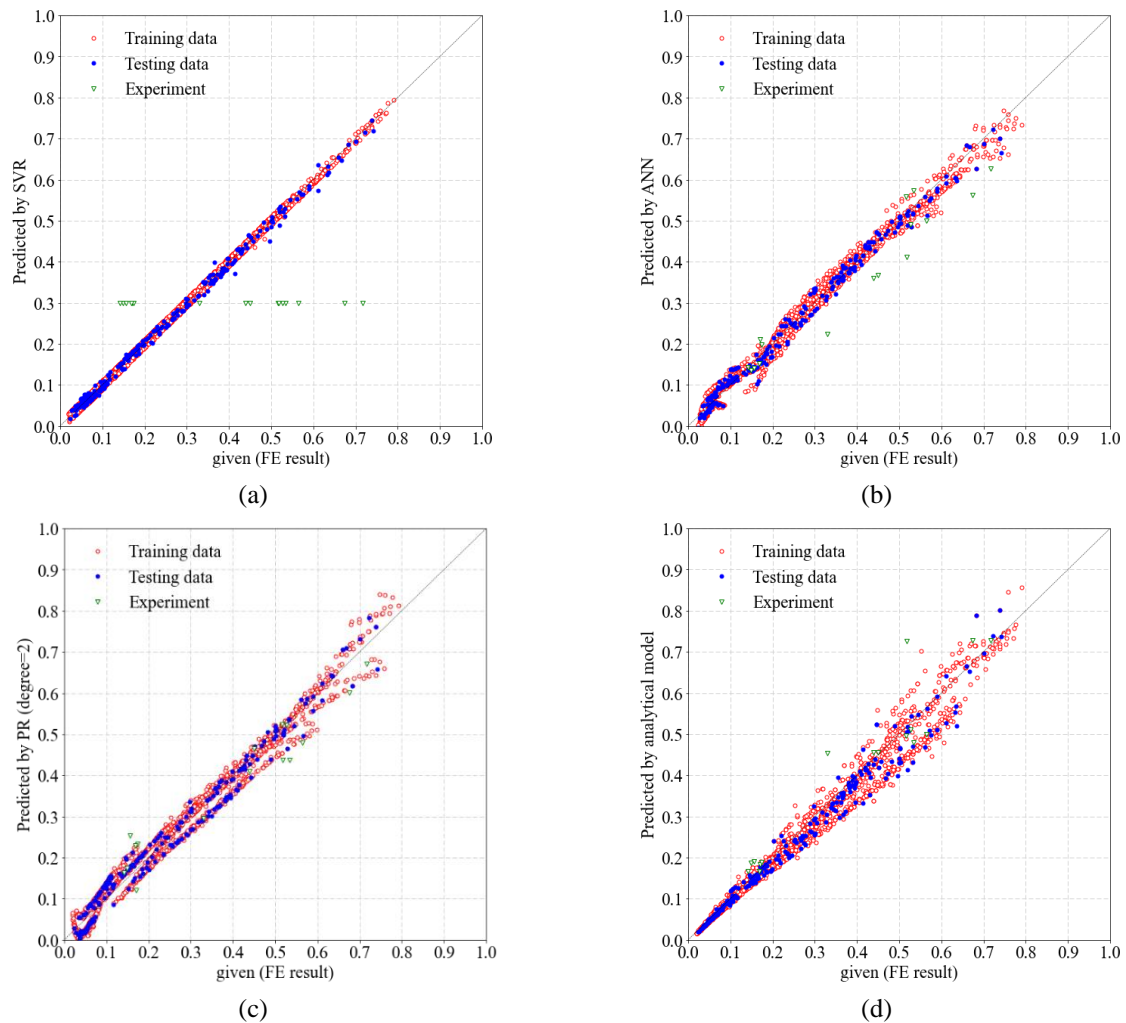


Figure 2. Predicted capacity $N_{u,T}/N_{pl,20}$ for slender steel columns at elevated temperature: Comparison between SAFIR finite element model and (a) SVR; (b) ANN; (c) PR; (d) Analytical model. Training/testing performed based on 2304 data points. “Experiment” refers to 16 experimental data points not used in the construction of the ML models.

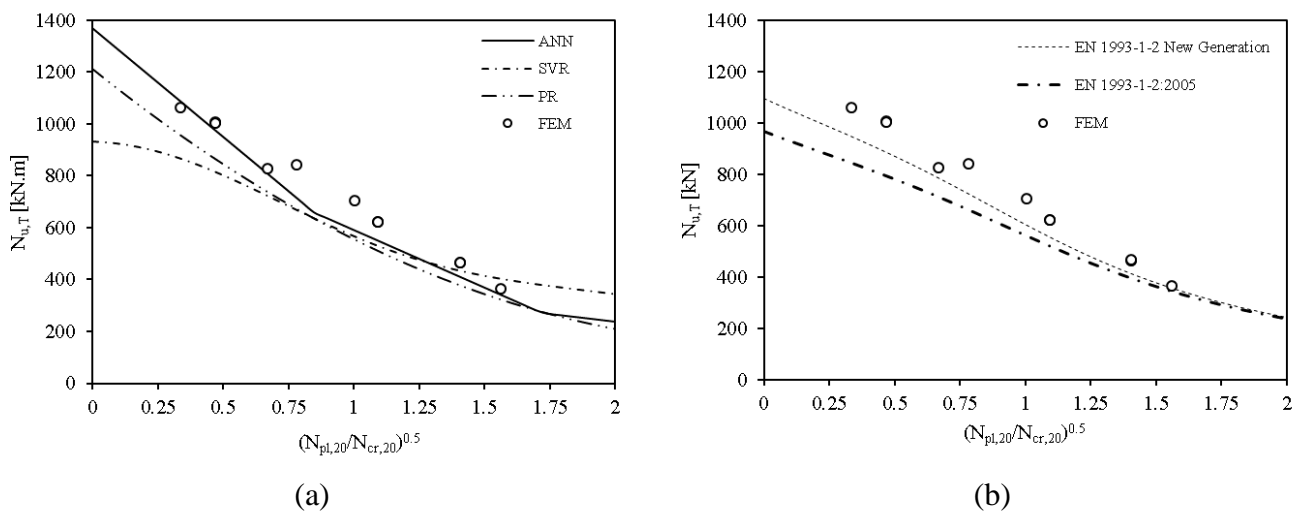


Figure 3. Comparison between numerical results (FEM) and (a) machine learning models or (b) analytical models for columns with cross section IPE A 300 (S460) at 500 °C.

In fact, when used to predict the outcome of the experiments from [13,14], which were not used to construct the models, the PR is the most accurate with R^2 of 0.914, followed by ANN, and the analytical model. The SVR model fails to capture the experimental data. The reason is the SVR is sensitive to the range of web slenderness and flange slenderness. Looking at the web and flange slenderness of the training, testing, and experimental data points (Table 1), reveals that the values of these features for the experimental data points fall outside of the range considered in the training and testing data points. When the web slenderness and flange slenderness are beyond the range of the trained model, the SVR fails to accurately extrapolate the outputs and the predictions of $N_{u,T}/N_{pl,20}$ are approximately constant at 0.3. This results from the high degree of nonlinearity of the SVR model. Attempts to improve the predictions with the SVR outside of the range of the parameters (to fit with the experimental data) were made, including by using a linear SVR or addressing the overfitting. However, any improvement of the performance against the experimental dataset was at the cost of a sensible reduction in performance against the training and testing datasets. Therefore, it was concluded that the nonlinear SVR model can provide high performance in the range of the training parameters, but should not be extrapolated outside this range.

For a different visualization of the results, Figure 3 shows the comparison of the different models for columns with IPE A 300 in S460 steel at 500 °C, as well as the numerical results obtained with the finite element model described in Section 2, considering different lengths of the column and different support conditions. In this figure, it is possible to observe the good correlation between the ML models and those obtained numerically. The shape of the curve obtained with the ANN might be explained by the number of lengths considered in the training set for the columns, by increasing this number a smoother curve would likely be obtained, as it is the case for the beams that are presented next.

For the beam cases, Figure 4 (a)-(d) plot the predicted capacity $M_{u,T}/M_{pl,20}$ using SVR, ANN, PR, and the analytical models against the numerical estimations from the shell finite element model in SAFIR. As for the columns, the different ML models for beams with slender section outperform the accuracy of the analytical methods defined in the future version of the EN 1993-1-2 which, in turn, provides already a better accuracy over its present version. The artificial neural network developed with *pyrenn* has reached R^2 scores of 0.999 on both the training and testing datasets thus provide an excellent choice to predict the capacity of thin-walled beams.

Figures 5 and 6 shows the comparison of different models for beams with cross-sections I450×4+150×12 and I450×4+200×10, made of S235 and S355 steels and subjected to a constant bending diagram ($\psi = 1$) and a triangular bending diagram ($\psi = 0$), respectively. The beams were calculated for 450 °C using the finite element model described in Section 2. For both sections, it is possible to observe the good correlation between the results predicted by the ML models and the results calculated numerically using the FEM. Regarding the analytical methods while it is noticeable the improvements of the new generation of EN1993-1-2 over the present version of the design code, as expected, both these methods present lower accuracy when compared against the ML models.

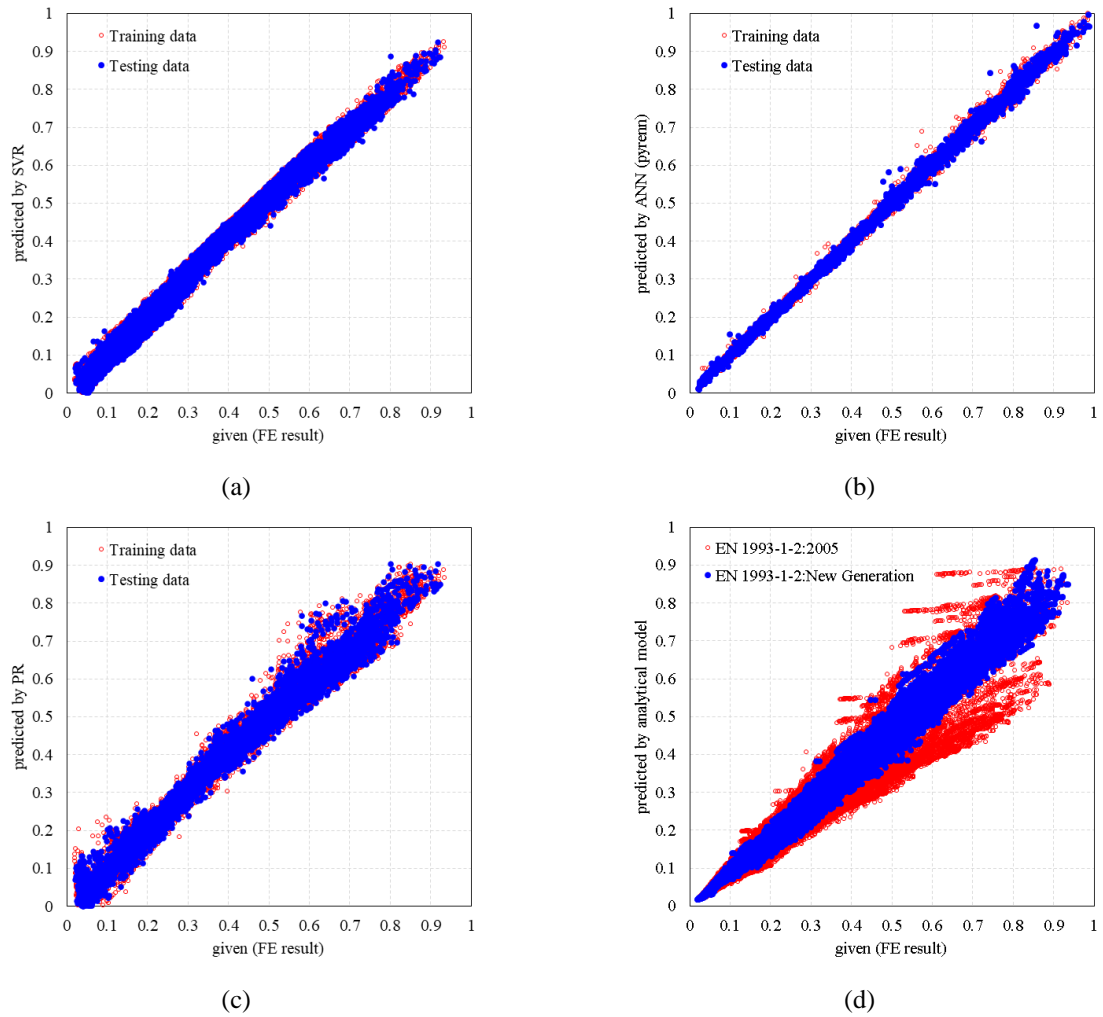


Figure 4. Predicted capacity $M_{u,T}/M_{pl,20}$ for slender steel beams at elevated temperature: Comparison between SAFIR finite element model and (a) SVR; (b) ANN; (c) PR; (d) Analytical models.

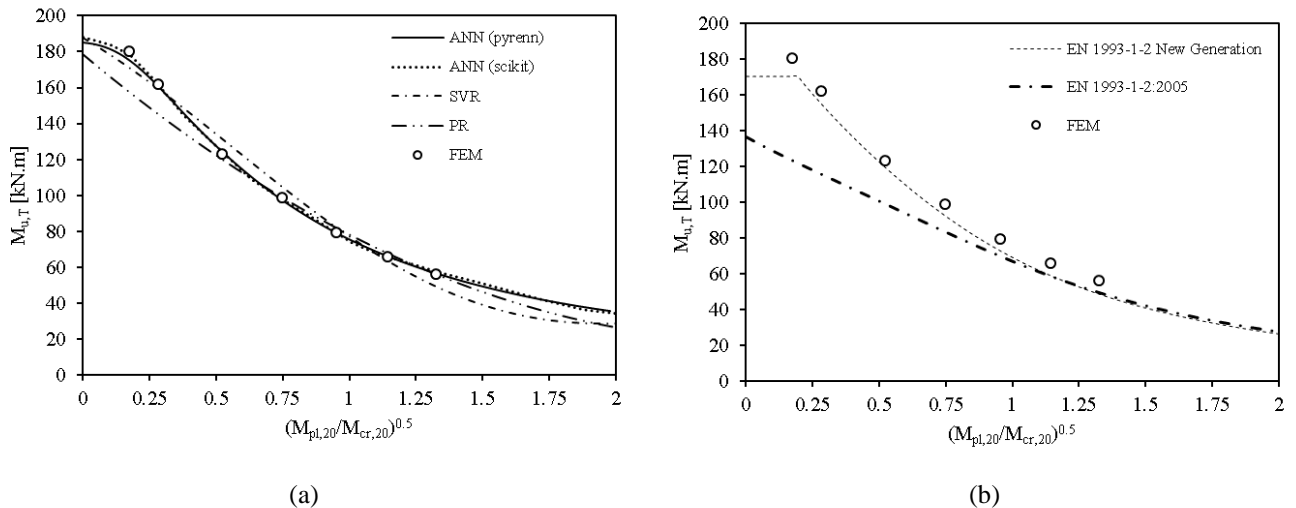


Figure 5. Comparison between numerical results (FEM) and (a) machine learning models or (b) analytical models for beams with cross section I450x4+150x12 (S235) at 450 °C and constant bending moment distribution ($\psi = 1$).

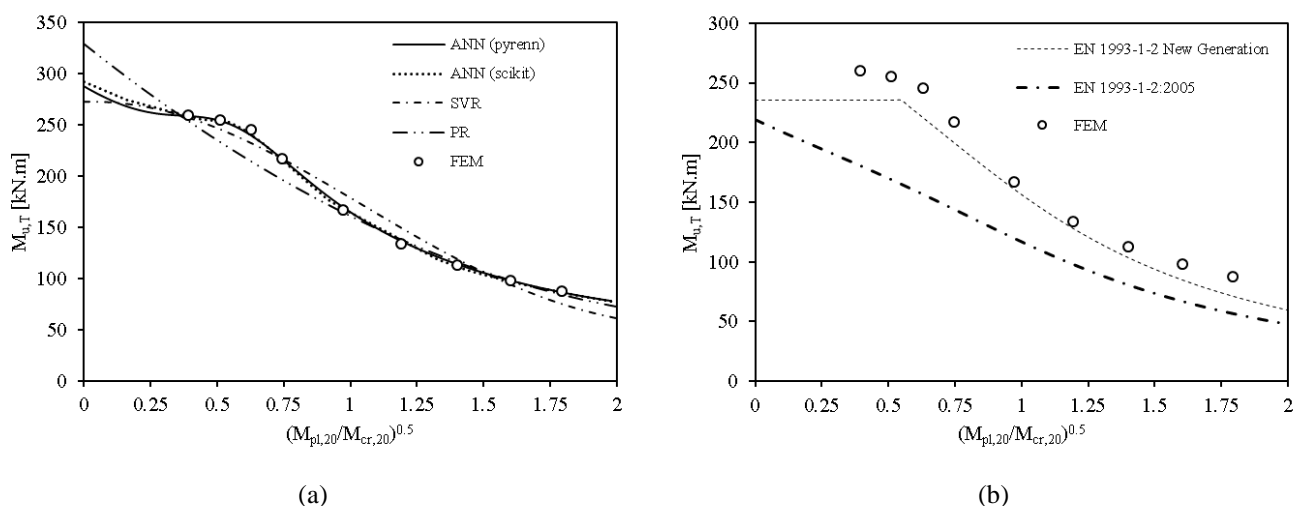


Figure 6. Comparison between numerical results (FEM) and (a) machine learning models or (b) analytical models for beams with cross section I450×4+200×10 (S355) at 450 °C and triangular bending moment distribution ($\psi = 0$).

6 CONCLUSION

This study investigated the potential of Machine Learning (ML) models to capture the capacity at elevated temperatures of steel members with slender sections which exhibit failure by local buckling and/or global buckling. A numerical study based on validated nonlinear FEM using shell elements was conducted to build a dataset of 2304 data points for columns and 24516 for beams with a range of cross-sections, member length, temperature, yield strength, and boundary conditions. The dataset was used to train and test ML models to predict the elevated temperature capacity of beams and columns. Three types of ML models were applied to the beam and column datasets separately, namely based on artificial neural network (ANN), support vector regression (SVR) and polynomial regression (PR).

For both the beams and columns, the ML models can fit the results of the shell FE models more closely than the state-of-the-art analytical methods to be included in the next generation of the Eurocodes. For columns, the ML models can predict the resistance at elevated temperature, for both the training and testing dataset, with a R^2 greater than 0.990 for SVR and ANN, and greater than 0.977 for PR. For beams, a R^2 greater than 0.981 is obtained for the PR, 0.987 for SVR and 0.999 for the ANN.

For the columns, the PR and ANN models were also able to capture experimental data not used to train the model and with inputs outside the range of the numerical training dataset with a R^2 of 0.914 and 0.891, respectively. The SVR model, while providing the best accuracy against the training and testing datasets, did not provide an acceptable agreement against the experimental data and should thus not be used for inputs outside of the range considered to build the model. It is expected that the accuracy against test data could be further improved by extending the training dataset for the ML models.

In addition, the representation of results in the form of buckling curves illustrates the ability of the ML models to capture the behaviour of the steel members across a large range of slenderness. Generally the ML models agreed better with the FE data than the state-of-the-art analytical models.

This work shows that ML models can accurately predict the resistance of both columns and beams under uniform heating while also being computationally efficient. Large numerical database that were developed as background to the development of analytical methods can be revisited to train ML models, following the procedure described in this paper. In future works, more complex configurations such as structural assemblies or non-uniform fire exposures will be explored.

ACKNOWLEDGMENTS

Carlos Couto acknowledges the funding from FCT – Fundação para a Ciência e a Tecnologia, I.P., under the Scientific Employment Stimulus – Institutional Call – CEECINST/00026/2018, and Rede Nacional de Computação Avançada (RNCA) da FCT, within the scope of the exploratory research project CPCA/A1/6717/2020.

Under a license agreement between Gesval S.A. and the Johns Hopkins University, Dr. Gernay and the University are entitled to royalty distributions related to the technology SAFIR described in the study discussed in this publication. This arrangement has been reviewed and approved by the Johns Hopkins University in accordance with its conflict of interest policies.

REFERENCES

1. Franssen JM, Cowez B, Gernay T. (2014). Effective stress method to be used in beam finite elements to take local instabilities into account. Proceedings of the 11th IAFSS Symposium (pp. 544-557). Christchurch, New Zealand, Feb 10-14. DOI: 10.3801/IAFSS.FSS.11-544.
2. Pallares-Muñoz MR, Payá-Zaforteza I, Hospitaler-Pérez A. New modeling strategies for analyzing lateral-torsional buckling in class-4 steel structural members at elevated temperatures using beam-type elements. Structures 2021;34:3508–32. <https://doi.org/10.1016/j.istruc.2021.09.087>.
3. Naser MZ. Mechanistically Informed Machine Learning and Artificial Intelligence in Fire Engineering and Sciences. Fire Technol 2021;57:2741–84. <https://doi.org/10.1007/s10694-020-01069-8>.
4. Franssen J, Gernay T. Modeling structures in fire with SAFIR ® : Theoretical background and capabilities. Journal of Structural Fire Engineering 2017;1–28. <https://doi.org/10.1108/JSFE-07-2016-0010>.
5. CEN. EN 1993-1-5, Eurocode 3 - Design of steel structures - Part 1-5: Plated structural elements 2006:1–53.
6. Couto C, Vila Real P, Lopes N, Zhao B. Resistance of steel cross-sections with local buckling at elevated temperatures. Journal of Constructional Steel Research 2015;109:101–14. <https://doi.org/10.1016/j.jcsr.2015.03.005>.
7. Couto C, Vila Real P, Lopes N, Zhao B. Numerical investigation of the lateral–torsional buckling of beams with slender cross sections for the case of fire. Engineering Structures 2016;106:410–21. <https://doi.org/10.1016/j.engstruct.2015.10.045>.
8. Couto C, Maia É, Vila Real P, Lopes N. The effect of non-uniform bending on the lateral stability of steel beams with slender cross-section at elevated temperatures. Engineering Structures 2018;163:153–66. <https://doi.org/10.1016/j.engstruct.2018.02.033>.
9. CEN. EN 1993-1-2, Eurocode 3: Design of steel structures - Part 1-2: General rules - Structural fire design 2005.
10. Couto C, Vila Real P. The influence of imperfections in the critical temperature of I-section steel members. Journal of Constructional Steel Research 2021;179:106540. <https://doi.org/10.1016/j.jcsr.2021.106540>.
11. Tong Q, Couto C, Gernay T. Machine learning models for predicting the resistance of axially loaded slender steel columns at elevated temperatures. Engineering Structures 2022;266:114620. <https://doi.org/10.1016/j.engstruct.2022.114620>.
12. Couto C, Tong Q, Gernay T. Predicting the capacity of thin-walled beams at elevated temperature with machine learning. Fire Safety Journal 2022;130:103596. <https://doi.org/10.1016/j.firesaf.2022.103596>.
13. Wang W, Kodur V, Yang X, Li G. Experimental study on local buckling of axially compressed steel stub columns at elevated temperatures. Thin-Walled Structures 2014;82:33–45. <https://doi.org/10.1016/j.tws.2014.03.015>.
14. Pauli J, Somaini D, Knobloch M, Fontana M. Experiments on steel columns under fire conditions - Test Report No. 340, 2012. , ETH Zurich, Institute of Structural Engineering IBK; 2012.
15. Pedregosa F, Varoquaux G, Gramfort A, Michel V, Thirion B, Grisel O, et al. Scikit-learn: Machine learning in Python. The Journal of Machine Learning Research 2011;12:2825–30.
16. Atabay D. pyrenn: A recurrent neural network toolbox for Python and Matlab. Institute for Energy Economy and Application Technology, Technische Universität, München.